



City Research Online

## City, University of London Institutional Repository

---

**Citation:** De, M., Markides, C., Singh, V. K., Themistos, C. & Rahman, B. M. (2020). Analysis of a Single Solid Core Flat Fiber Plasmonic Refractive Index Sensor. *Plasmonics*, 15(5), pp. 1429-1437. doi: 10.1007/s11468-020-01154-2

This is the accepted version of the paper.

This version of the publication may differ from the final published version.

---

**Permanent repository link:** <https://openaccess.city.ac.uk/id/eprint/24787/>

**Link to published version:** <https://doi.org/10.1007/s11468-020-01154-2>

**Copyright:** City Research Online aims to make research outputs of City, University of London available to a wider audience. Copyright and Moral Rights remain with the author(s) and/or copyright holders. URLs from City Research Online may be freely distributed and linked to.

**Reuse:** Copies of full items can be used for personal research or study, educational, or not-for-profit purposes without prior permission or charge. Provided that the authors, title and full bibliographic details are credited, a hyperlink and/or URL is given for the original metadata page and the content is not changed in any way.

---

---

---

City Research Online:

<http://openaccess.city.ac.uk/>

[publications@city.ac.uk](mailto:publications@city.ac.uk)

---

# Analysis of a single solid core flat fiber plasmonic refractive index sensor

Moutusi De<sup>1\*</sup>, Christos Markides<sup>2</sup>, Vinod Kumar Singh<sup>1</sup>, Christos Themistos<sup>2</sup>  
and B. M. A. Rahman<sup>3</sup>

<sup>1</sup>Department of Physics, IIT (ISM) Dhanbad, India

<sup>2</sup>Department of Electrical Engineering, Computer Engineering and Informatics, Frederick  
University, Nicosia, Cyprus

<sup>3</sup>Department of Electrical and Electronic Engineering, City University of London, UK

\*E-mail: [moutusi.2016dr0011@ap.ism.ac.in](mailto:moutusi.2016dr0011@ap.ism.ac.in)

**Abstract:** In this article, a single solid core flat fiber (SSCFF) refractive index sensor based on surface plasmon resonance (SPR) is proposed and analysed numerically using the finite element method (FEM). The proposed flat fiber consists of a single array of five circular holes. Among them the central hole is made of GeO<sub>2</sub> doped silica which is forming the core. Other holes are filled with air and situated symmetrically on both sides of the central solid core. The upper flat surface of the fiber is coated with a thin plasmonic gold layer which is protected by an active titanium dioxide layers. Analyte is situated on top of these layers. The wavelength interrogation technique is applied to study the coupling characteristics between the core guided mode and the surface plasmon mode as well as for the refractive index measurement. Numerical analysis results show that this sensor is able to detect high refractive index analytes from 1.49 to 1.54 with a good linear response. Additionally, the dependence of surface plasmonic resonance wavelength on analyte refractive index is studied. The maximum wavelength sensitivity of this sensor is found to be 4782 nm/RIU with a high resolution of  $2.09 \times 10^{-5}$  RIU. The effects of different structural parameters on loss spectrum are studied in detail to optimize this SSCFF structure. In comparison to traditional PCF, this SSCFF structure is fabrication complexity free as well as a suitable candidate for developing portable devices, high refractive index analyte sensors, particularly chemical and protein sensors.

Keywords: Optical sensing, photonic crystal fiber, refractive index sensor, surface plasmon, finite element method.

## **1. Introduction:**

The exponentially increasing demand for portable high sensitive sensors has given a new boost to the development of Surface plasmon resonance (SPR) based sensor technology. The SPR is a unique phenomenon in which electromagnetic wave is trapped between a single metal-dielectric interface. Also, energy is transferred from p-polarized light to free electrons at metal-dielectric interface via evanescent waves. SPR takes place at a particular frequency when the frequency of propagating light matches with the oscillating frequency of free electrons at the metal-dielectric interface. Then surface plasmon wave (SPW) propagates along the metal-dielectric interface [1, 2]. The nearby environment influences this trapped electromagnetic wave as well as the coupling condition; i.e., the SPR wavelength experiences a noticeable shift with the change of surrounding refractive index (RI) [3, 4]. These characteristic properties are encouraging many research groups in developing SPR based high sensitive RI sensors. Apart from RI monitoring, SPR based sensors have potential applications in chemistry, bioscience, food safety, medicine, environmental monitoring, to name a few, due to its highly sensitive nature and label-free sensing ability [2, 5–7].

For the first time, in 1968, a prism based SPR technique [Kretschmann-Raether configuration] was reported. In this configuration, a prism surface is coated with plasmonic material and applied for sensing due to its structural simplicity and ease of fabrication [8]. However, due to its bulk size, robustness, and incompatibility in remote sensing this structure did not gain much attention. To overcome these limitations, in 1993 Jorgenson successfully demonstrated an optical fiber SPR sensor [9]. Then several innovative steps are taken toward developing optical waveguide using SPR sensors. Such as, single-mode fiber [10], multi-mode fiber [11], microring resonator [12], fiber Bragg grating [13], long-period grating [14], plasmonic metal nanostructure [15, 16], microstructured fiber [2] etc are used for the fabrication of SPR sensors. In many cases, these sensors suffer from sensitivity and detection accuracy limitations. For instance, the SPR peak experience a low wavelength shift with changing environment. On the other hand, photonic crystal fibers (PCFs) have many desirable optical properties like small size, less material selection

complexity, endlessly single mode propagation, high birefringence, ultra-flattened dispersion, tunable confinement loss, immunity in harsh environment and most importantly excellent design flexibility with the power of manipulating propagating light as per requirement [17–19]. Moreover, selectively infiltrated and internally plasmonic thin film coated PCF based SPR sensors are reported [20–22], but this kind of fabrication is not easy in practice. Also, it is time consuming and challenging to produce on a large scale with the existing technology.

D-shape PCFs overcome many of these limitations. In D-shaped fiber, a portion of the fiber is side polished and plasmonic metals are deposited on top of it to generate SPW. In 2012, a silver layer coated all solid D-PCF is proposed for analyte sensing by Tian *et al.*[23]. Also, Luan *et al.* reported a thin gold layer incorporated D-shape hollow core microstructured optical fiber (MOF) PCF-based SPR sensor having sensitivity 2900 nm/RIU [24]. They also reported a unique gold coated D-shaped PCF SPR sensor with a laterally accessible hollow core for low RI analyte sensing [25]. Dash *et al.* reported a silver-graphene coated birefringent D-PCF for analyte sensing [26]. The same group proposed graphene using PCF bilayer sensor having sensitivity 3700 nm/RIU [27]. So far, many D-PCF SPR sensors have been reported with different internal air hole distribution and plasmonic layer coating. Many of these D-PCF have complicated internal structures to manipulate evanescent waves towards the polished surface. Also, the predetermined polishing of the PCF is required in order to obtain proper light coupling between the core mode and the SPP mode.

Optical fiber has its advantages in making portable remote sensors. These advantages are promoted in a more effective way when the fiber takes the form of a planar waveguide. Planar waveguide sensors are advantageous in many aspects like, larger sensing area, faster response, more accuracy, compatibility with fiber optic network, imperviousness to EM interference, etc. In this aspect, asymmetric planar waveguides are crucial in current research [28]. In 2005, a flat fiber was demonstrated for developing a fiber laser, named as multicore ribbon fiber [29]. In the last decade, Mahdiraji *et al.* [30] and Egorova *et al.* [31] reported a few flat fibers for accommodating multiple waveguide channels. In 2016, Rifat *et al.* proposed a multi-core flat fiber based SPR sensor [22], in which two alternative air holes are filled with high RI analyte to form twin core and again the same analyte is placed on the top. Although the reported fiber has a large sensing area, as well as high sensitivity, it is not free from void infiltration problems and poor linearity. Also, during

analysis inter coupling between these two core are not taken into account. To overcome these limitations and to fully utilize the advantages of flat fiber, a unique single solid core flat fiber (SSCFF) based SPR sensor is proposed in this article. The structure is optimized based on structural parameters like, pitch, hole diameter and deposited layers thickness. This SSCFF is used to detect analytes from 1.49 to 1.54 RIU. The optimized structure shows maximum wavelength sensitivity of 4782 nm/RIU with high resolution  $2.09 \times 10^{-5}$  RIU. This SSCFF operates in the near-infrared wavelength region. It is believed that the proposed SSCFF is feasible in fabricating portable devices capable of measuring high RI analyte.

## **2. Working principle:**

In a PCF light is guided not only by the refractive index difference but also by the internal structure. For a PCF using SPR sensor, the optimized internal air hole distribution also promotes the effective interaction between evanescent wave and analyte. In this SSCFF, light is propagating along z-direction via total internal reflection and modal investigation is performed in the xy plane. The linear core-cladding arrangement yields substantial evanescent field leakage from the core [32]. Exciting free electrons are generated between the analyte and gold layer via leaked evanescent field from the core towards the analyte layer. At a particular propagating wavelength, the real effective refractive index ( $\text{Re}(n_{\text{eff}})$ ) of the fundamental core mode and the surface plasmon (SP) mode are equal. It is known as surface plasmon resonance (SPR) wavelength. At the SPR wavelength, evanescent field significantly excite free electrons at metal-dielectric interface and prominent interaction takes place between sprface plasmon wave and analyte. At the SPR wavelength, a peak appears in loss spectra of the core guided mode due to the maximum energy transfer from the core to the SP mode. In this analysis, the 1<sup>st</sup> order SP mode is considered because fundamental SP mode couples with the core mode far away from the near-infrared region.

## **3. SSCFF sensor structure design and numerical modelling:**

The cross-sectional view and three dimensional probe structure of the proposed SSCFF are shown in Fig. 1(a) and Fig. 1(b) respectively. The proposed SSCFF structure consists of a single array of five holes. The central hole is made of 13.5% GeO<sub>2</sub> doped silica and forms the core to guide light. Light is propagating through this fiber based on the total internal reflection principle. On either side of the core there are two air holes in a linear position to guide light as well as to minimize

leakage losses. Diameter of all air holes and the core are same. The background material of this structure is silica.

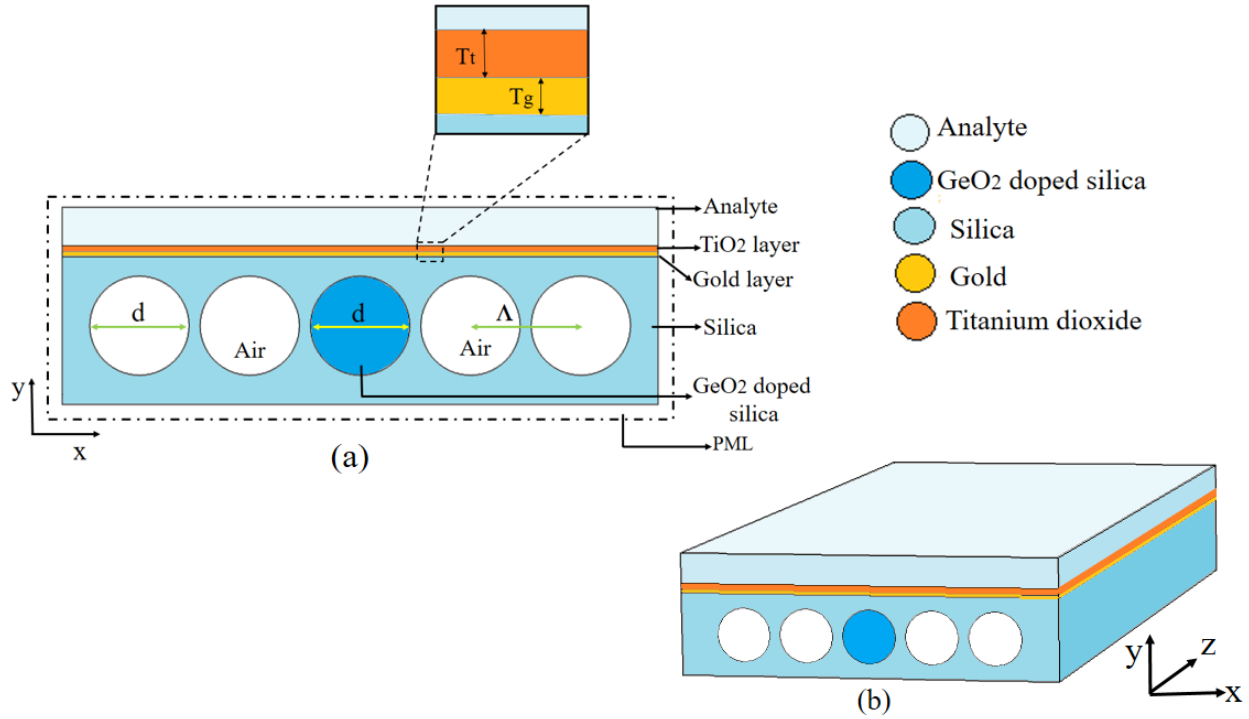


Fig. 1(a) Schematic cross-sectional view ( $xy$  plane) of the SSCFF and (b) 3D structure of SSCFF.

On the upper surface of the flat fiber there is a thin gold (Au) layer, which is deposited as plasmonic metal to generate the SPW. Noble metal, Au is a chemically stable material and has a sharp loss peak at the SPR frequency [2, 25, 32]. A relatively thicker titanium dioxide ( $\text{TiO}_2$ ) layer is deposited on top of the gold layer. This high refractive and transparent  $\text{TiO}_2$  layer helps in coupling the evanescent field of propagating light from core to the analyte. Also, the  $\text{TiO}_2$  layer brings down the SPR wavelength in the near-infrared region, which reduces the problem of selecting a suitable light source and a detector. Also higher penetration takes place in near infrared region in comparison to the visible region which enhances the sensitivity [2, 33, 34]. For the practical realization of this sensor, a thin ( $\leq 5\text{nm}$ )  $\text{TiO}_2$  layer can be incorporated in between silica and gold layers for better adhesion. Although adhesion by  $\text{TiO}_2$  layer is relatively weaker in comparison to the commonly used Cr and Ti coating [35]; but it helps in spectral tuning of the SPR wavelength, unlike Cr and Ti coating [36]. To reduce the computational time this adhesive  $\text{TiO}_2$  layer is taken into account as a part of the upper  $\text{TiO}_2$  tuning layer. The sensing layer is situated on the top of  $\text{TiO}_2$  layer. Refractive index of the sensing layer ( $n_a$ ) is varied from 1.49 to 1.54. For the proposed

SSCFF structural parameters are as follows, pitch ( $\Lambda$ ), air hole/core diameter ( $d$ ), gold layer thickness ( $T_g$ ),  $TiO_2$  layer thickness ( $T_t$ ), where the refractive index of air is 1. The optimization process is discussed in section 4.1. Material dispersion of silica is considered by following the Sellmeier equation,

$$n^2(\lambda) = 1 + \frac{A_1\lambda^2}{\lambda^2 - B_1} + \frac{A_2\lambda^2}{\lambda^2 - B_2} + \frac{A_3\lambda^2}{\lambda^2 - B_3} \quad (1)$$

Here,  $\lambda$  is the propagating wavelength. Sellmeier coefficients of background material (silica) and  $GeO_2$  doped silica are taken into account based on Brückner's report [37].

The complex dielectric constant of Au is incorporated in this simulation using the Johnson and Christy data [29,32].

When  $\lambda$  is measured in  $\mu m$ . The dispersion relation of  $TiO_2$  is as follows [33],

$$\epsilon_{TiO_2} = 5.913 + \frac{0.2441}{\lambda^2 - 0.0843} \quad (2)$$

Loss of the core guided mode can be calculated using following equation [25],

$$\alpha = 8.686 \times \frac{2\pi}{\lambda} \text{Im}(n_{\text{eff}}) \times 10^4 \text{ (dB/cm)} \quad (3)$$

here,  $\text{Im}(n_{\text{eff}})$  is the imaginary part of the effective refractive index ( $n_{\text{eff}}$ ).

FEM based commercial COMSOL Multiphysics software (4.4 version, RF module) [39] is used to study the designed SSCFF sensor. A PML layer of thickness  $1\mu m$  is applied around the fiber as a boundary condition. It reduces the radiation loss from the fiber. The cross section of this fiber is meshed into 'extra fine' triangulate elements. Then Maxwell's electromagnetic equations are applied to each element. 5535 domain elements, 856 boundary elements and 35581 degrees of freedom are solved during the simulation.

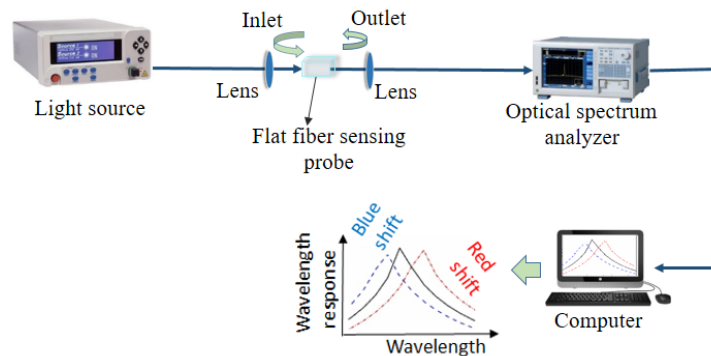


Fig. 2 Schematic diagram of the experimental setup

This simple flat fiber structure is used for developing a SPR sensor because of its large surface area; as a result, active interaction with the surroundings. In addition, this fiber has a single solid core with a conventional RI profile. For this structure, considered GeO<sub>2</sub> doped silica core is compatible with the silica background [37]. The plasmonic layer and TiO<sub>2</sub> layer are deposited on top of the fiber without selective coating complexity. Due to the structural simplicity this SSCFF sensor is easy to fabricate. For this SSCFF structure, all five internal holes including the core have the same diameter. Thus, the flat fiber can be fabricated using the suspended array drawing method at the presence of pressure [30], stack and draw based fiber fabrication technology [31], as well as the modified powder- in-tube technique [40]. A thin Au layer and TiO<sub>2</sub> layer can be deposited by the sputtering technique [41] and the chemical method [42, 43] respectively. Light can be launched at the input end of the sensing probe as well as can be channelized to the spectrum analyzer by using free-space coupling [44]. A suggested experimental set up is shown in Fig. 2. A minimal amount of sample has to be poured on top of the SSCFF sensing probe to detect a suspected analyte.

#### 4. Results and discussion:

Modal analysis are performed on the cross section of the fiber i.e. in xy plane. Here, it is considered that unpolarised light is propagating through the fiber along z direction. There are two fundamental core guided modes, namely x-polarized core mode (H<sub>x</sub>) and y-polarized core mode (H<sub>y</sub>). Through out the study, y polarized mode is considered for loss and sensitivity investigation because the plasmonic layer is situated in y-direction. So, y polarized light gives better interaction between evanescent wave and Au layer in comparison to x polarized mode [25, 27]. Loss of core guided fundamental mode ( $\alpha$ ) can be calculated using Eq. (3).

##### 4.1 Performance optimization:

Fig. 3-6 depict the loss spectrum variation with changing  $\Lambda$ , d, T<sub>g</sub> and T<sub>t</sub>. To optimize the SSCFF structure one parameter is varied at a time. Fig. 3 shows loss variations with changing  $\Lambda$  for d=1.80  $\mu\text{m}$ , T<sub>g</sub>=40 nm, T<sub>t</sub>=80 nm and n<sub>a</sub>=1.50. For increasing  $\Lambda$  from 1.85  $\mu\text{m}$  to 2.10  $\mu\text{m}$  with an iteration of 0.5  $\mu\text{m}$  loss peak shifts towards the longer wavelength with decreasing loss peak. For  $\Lambda$ =1.85  $\mu\text{m}$  maximum loss is found at 1.258  $\mu\text{m}$  wavelength. The core mode gets compressed side-wise with decreasing  $\Lambda$ . As a result, more propagating light gets coupled towards the plasmonic layer and more core loss takes place. It is also observed that with decreasing pitch ( $\Lambda$ ) sensitivity (Eq. (5)) increases continuously. The highest sensitivity 3556 nm/RIU is obtained for  $\Lambda$ =1.85  $\mu\text{m}$ .

Considering both the spectral scalability and ease of light leakage through the passages  $\Lambda$  is chosen at a higher value in comparison to the operating wavelength. So,  $1.85 \mu\text{m}$  is the optimized pitch. Then, the hole diameter ( $d$ ) is varied from  $1.72$  to  $1.80 \mu\text{m}$  with a step of  $0.02 \mu\text{m}$ , where  $\Lambda$ ,  $T_g$ ,  $T_t$  and  $n_a$  are  $1.85 \mu\text{m}$ ,  $40 \text{ nm}$ ,  $80 \text{ nm}$  and  $1.50$  respectively. In this case, loss peak experiences blue shift as shown in Fig. 4. For  $d=1.76 \mu\text{m}$ , the highest loss is found at  $1.269 \mu\text{m}$  wavelength. Also, at this hole diameter for  $\Delta n_a=0.01$  the sensitivity is found to be  $3122 \text{ nm/RIU}$ . The variation of hole diameter affects the electric field distribution, leakage of propagating light as well as the surface plasmon (SP) wave. It is observed that with increasing  $d$  sensitivity also increases. The reason behind this is for bigger air holes the evanescent field is driven more toward the plasmonic layer as a result more interaction with the analyte. However, this in turn affects the robustness of the fiber. So, considering these facts  $1.76 \mu\text{m}$  is chosen as the optimized hole diameter.

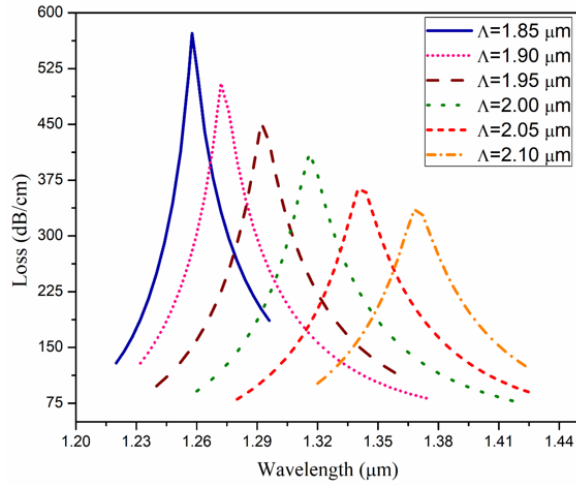


Fig. 3

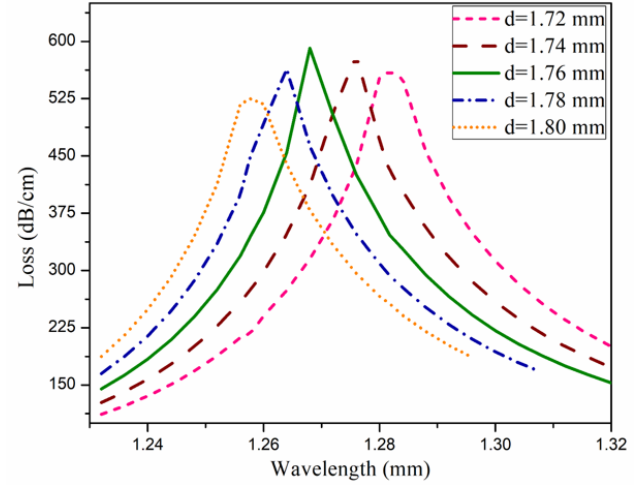


Fig. 4

Fig. 3 Loss curves with changing wavelength as a function of pitch [ $\Lambda$ ] with  $d=1.80 \mu\text{m}$ ,  $T_g=40 \text{ nm}$  and  $T_t=80 \text{ nm}$ . Fig. 4 Loss curves with changing wavelength as a function of hole diameter [ $d$ ] with  $\Lambda=1.85 \mu\text{m}$ ,  $T_g=40 \text{ nm}$  and  $T_t=80 \text{ nm}$ .

Response of a SPR sensor is strongly dependent on the plasmonic layer thickness as SP waves are sensitive to this layer. So, during the optimization of the proposed SSCFF structure effect of gold layer thickness ( $T_g$ ) is studied.  $T_g$  is varied from  $35 \text{ nm}$  to  $50 \text{ nm}$  with an iteration of  $5 \text{ nm}$  where  $\Lambda=1.85 \mu\text{m}$ ,  $d=1.76 \mu\text{m}$ ,  $T_t=80 \text{ nm}$  and  $n_a=1.50$ . Fig. 5 shows loss variations with changing gold layer thickness. For the  $45 \text{ nm}$  thick gold layer maximum loss is observed with a sharp peak at a wavelength of  $1.244 \mu\text{m}$ . Also, for this  $T_g$  the sensitivity is found to be  $3297 \text{ nm/RIU}$ . From Fig. 5 it can be observed that on both side of  $T_g=45 \text{ nm}$  loss is less. The reason of this can be explained

as, two type of damping work on the SP wave one is mechanical damping and another is plasmonic damping. When gold layer is too thin then mechanical damping is dominant. On the other hand, when gold layer is too thick then plasmonic damping is dominant. Also from the background study it is found that with decreasing  $T_g$  sensitivity suffers decrement [25]. Considering all this aspects 45 nm is chosen as the optimized gold layer thickness for this SSCFF sensor.

Then the effect of  $TiO_2$  layer thickness ( $T_t$ ) on core mode loss is investigated. It is observed that both coupling strength and sensitivity got strongly effected with changing  $T_t$ . Fig. 6 shows a blue shift of SPR wavelength with increasing  $T_t$  from 70 nm to 90 nm with a step of 5 nm here other parameters  $\Lambda$ ,  $d$ ,  $T_g$  and  $n_a$  are kept constant at 1.85  $\mu m$ , 1.76  $\mu m$ , 45 nm and 1.50 respectively. It is observed that loss peaks suffer decrement with increasing  $T_t$ . The reason behind this is the evanescent field is screened from the analyte for a thicker  $TiO_2$  layer. Also from the background study it is found that sensitivity experiences a continuous increment with increasing high refractive  $T_t$ .

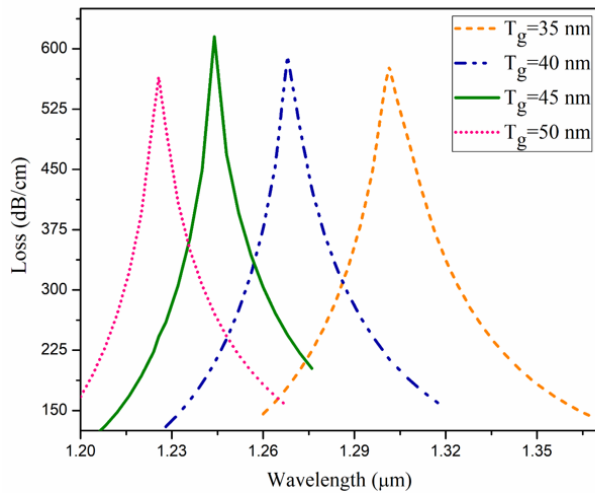


Fig. 5

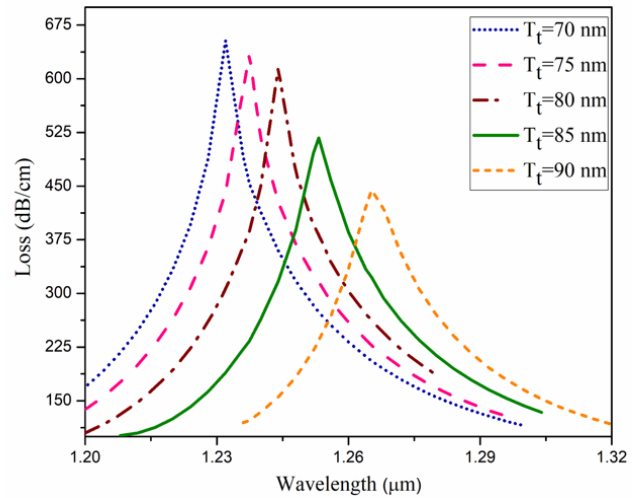


Fig. 6

Fig. 5 Loss curves with changing wavelength as a function of gold layer thickness [ $T_g$ ] with  $\Lambda=1.85 \mu m$ ,  $d=1.76 \mu m$  and  $T_t=80 nm$ . Fig. 6 Loss curves with changing wavelength as a function of  $TiO_2$  layer thickness [ $T_t$ ] with  $\Lambda=1.85 \mu m$ ,  $d=1.76 \mu m$  and  $T_g=45 nm$ .

So, considering both these facts 85 nm is chosen as an optimized  $TiO_2$  layer thickness. For this  $T_t$  sensitivity is found to be 4171 nm/RIU with a moderate loss. In addition, this layer can also act as a protective layer. Based on the rigorous study, optimized structural parameters for this SSCFF are chosen as  $\Lambda=1.85 \mu m$ ,  $d=1.76 \mu m$ ,  $T_g=45 nm$  and  $T_t=85nm$  respectively.

#### 4.2 Response of the proposed SSCFF probe:

The optimized SSCFF structure is applied for the modal analysis with changing analyte. In Fig.7, blue triangles consisting line depicts the  $\text{Re}(n_{\text{eff}})$  variation of core guided mode with changing wavelength. This mode is less lossy (inset Fig. b). In the same figure, blue squares consisting line shows the  $\text{Re}(n_{\text{eff}})$  variation of SP mode with changing wavelength. This mode is more dispersive and relatively more lossy (inset Fig. a) in comparison to the core mode. Both of these curves intersect at  $1.253 \mu\text{m}$  wavelength. This particular wavelength is the SPR wavelength. At SPR wavelength when both core mode and SP mode have same  $\text{Re}(n_{\text{eff}})$  and resonance takes place, then core mode becomes very lossy (inset Fig. c), which is indicated by the red arrow. In Fig. 7, core loss curve is depicted by red circle consisting line.

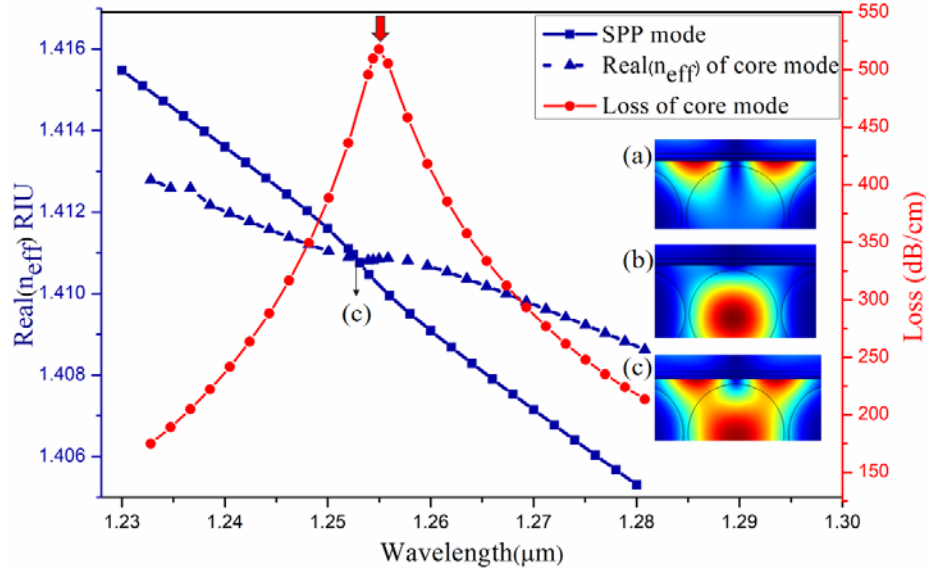


Fig. 7 Dispersion relations of the core guided mode (blue line with triangle) and plasmonic mode (blue line with square), loss curve of core mode (red line with circle) for proposed SSCFF sensing probe with structural parameters  $\Lambda=1.85 \mu\text{m}$ ,  $d=1.76 \mu\text{m}$ ,  $T_g=45 \text{ nm}$ ,  $T_t=85 \text{ nm}$  and  $n_a=1.50$ .

Fig. 8 depicts the loss curve variation with changing RI of analyte from 1.49 to 1.54 with an iteration of 0.01. A small amount of change in analyte RI causes a noticeable shift in the loss spectrum, as the SP mode is strongly dependent on the surroundings environment. From Fig. 8, it can be observed that with increasing  $n_a$  the SPR wavelength suffers a redshift (indicated by a red arrow). The reason behind this is when  $n_a$  increases,  $n_{\text{eff}}$  of SP mode also increases. As a result intersection between the core mode and SP mode takes place at a higher wavelength. For analyte

RI 1.49, 1.50, 1.51, 1.52, 1.53 and 1.54 associate losses at their respectively SPR wavelengths are 617, 505, 328, 231, 181 and 153 dB/cm.

#### 4.3 Wavelength interrogation and sensitivity:

For the optimized SSCFF structure, SPR peak shift with changing analyte is depicted in Fig. 9. Its  $R^2$  value is 0.991 i.e. the SPR peak suffers almost linear shift with changing  $n_a$  from 1.49 to 1.54.

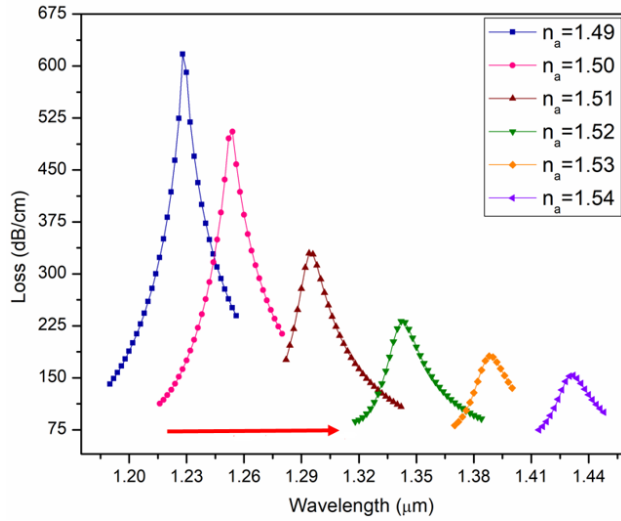


Fig. 8

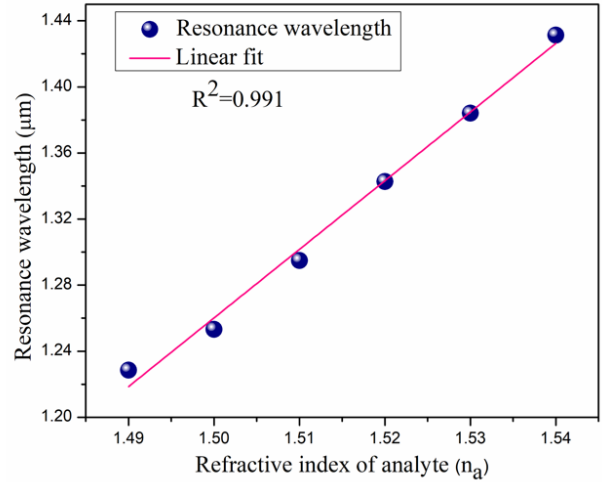


Fig. 9

Fig. 8 Loss spectrum of proposed SSCFF with changing analyte RI from 1.49 to 1.54, Fig. 9 SPR peak shift with changing analyte ( $n_a$ ) for optimized SSCFF structure.

The relation between the SPR peak position and  $n_a$  can be presented by the linear equation as follows,

$$\lambda_{\text{peak}}(n_a) = 4.15575 n_a - 4.97351 \quad (4)$$

The sensitivity of this SSCFF sensor can be calculated by using the wavelength interrogation method as follows [1, 25],

$$S = \frac{\Delta\lambda_{\text{peak}}}{\Delta n_a} \text{ nm/RIU} \quad (5)$$

Also, the resolution can be calculated using the following equation,

$$R = \Delta n_a \times \frac{\Delta\lambda_{\text{min}}}{\Delta\lambda_{\text{peak}}} \text{ RIU} \quad (6)$$

Here,  $\Delta\lambda_{\text{peak}}$  is the SPR peak shift,  $\Delta n_a$  is associated analyte RI change and minimum spectral resolution ( $\Delta\lambda_{\text{min}}$ )=0.1 nm [22, 25].

The performance of this SSCFF sensor is summarized in Table 1. The average wavelength sensitivity of this sensor is found to be 4156 nm/RIU. Also, the maximum wavelength sensitivity

of this sensor is 4782 nm/RIU when  $n_a=1.51$  and its corresponding resolution is  $2.09 \times 10^{-5}$  RIU. It shows that this sensor is capable of detecting analyte change of the order of  $10^{-5}$ .

Table 1 Performance of the SSCFF sensor for analyte variation

$n_a$ (RIU)	Resonance wavelength ( $\lambda_{peak}$ ) ( $\mu\text{m}$ )	Resonance peak shift (nm) (approx.)	Sensitivity (nm/RIU)
1.49	1.228	25	2474
1.50	1.253	42	4171
1.51	1.295	48	4782
1.52	1.343	45	4566
1.53	1.388	43	4290
1.54	1.431	-	-

The performance of the proposed SSCFF sensor is compared with previously reported sensors in Table 2.

Table 2 Performance comparison of proposed SSCFF

Sensor structure	Report year	RI range (RIU)	Sensitivity (nm/RIU)	Resolution (RIU)	Ref.
Hollow core D shaped microstructure fiber	2015	1.33-1.34	2900	-	[24]
Graphene based D shaped PCF	2015	1.33-1.37	3700	$2.70 \times 10^{-5}$	[27]
Copper-graphene based PCF	2016	1.33-1.37	2000	$5.00 \times 10^{-5}$	[45]
Four big channel consisting PCF	2016	1.63-1.79	3233	$3.09 \times 10^{-5}$	[46]
Externally gold layer coated PCF	2017	1.33-1.37	4000	$2.50 \times 10^{-5}$	[20]
D shaped PCF based on gold grating	2018	1.36-1.38	3340	-	[3]
Hollow core silver coated PCF	2018	1.36-1.37	4200	$2.38 \times 10^{-5}$	[21]
<i>Single solid core flat fiber</i>	<i>2019</i>	<i>1.49-1.54</i>	<i>4782</i>	<i><math>2.09 \times 10^{-5}</math></i>	<i>This Work</i>

## 5. Conclusion

In this article, a single solid core flat fiber (SSCFF) sensor is designed and analysed in detail using the FEM. The structure is optimized based on structural parameters using wavelength interrogation technique. This simple structured sensor responds well in the analyte refractive index range from 1.49 to 1.54 with excellent linearity. It exhibits maximum wavelength sensitivity of 4782 nm/RIU with resolution  $2.09 \times 10^{-5}$  RIU. Promising features of this sensor make it suitable for fabricating portable devices, remote sensors as well as to be integrated with the lab-on-a-fiber technology.

## Acknowledgements

This work is supported by Frederick University under the EM LEADERS doctoral exchange program. Specifically, Moutusi De is grateful to Dr. Kyriacos Kalli, Associate Professor at Cyprus University of Technology, Cyprus for the valuable discussion. Authors are also thankful to Indian Institute of Technology (ISM), Dhanbad, India for providing partial simulation facilities for this work.

## References

1. Huang T (2017) Highly sensitive SPR sensor based on D-shaped photonic crystal fiber coated with indium tin oxide at near-infrared wavelength. *Plasmonics* 12:583–588. <https://doi.org/10.1007/s11468-016-0301-7>
2. Hu DJJ, Ho HP (2017) Recent advances in plasmonic photonic crystal fiber: design, fabrication and applications. *Adv Opt Photonics* 9:257–314. <https://doi.org/10.1364/AOP.9.000257>
3. Lu JGJ, Li Y, Han Y, Liu Y (2018) D-shaped photonic crystal fiber plasmonic refractive index sensor based on gold grating. *Appl Opt* 57:5268–5272. <https://doi.org/10.1364/AO.57.005268>
4. De M, Gangopadhyay TK, Singh VK (2019) Prospects of Photonic Crystal Fiber as Physical Sensor: An Overview. *Sensors* 19:464. <https://doi.org/10.3390/s19030464>
5. Zhao Y, Deng ZQ, Li J (2014) Photonic crystal fiber based surface plasmon resonance chemical sensors. *Sensors Actuators, B Chem* 202:557–567. <https://doi.org/10.1016/j.snb.2014.05.127>
6. Lu J, Stappen TV, Spasic D, Delport F, Vermeire S, Gils A, Lammertyn J (2016) Fiber optic-SPR platform for fast and sensitive infliximab detection in serum of inflammatory bowel disease patients. *Biosens Bioelectron* 79:173–179. <https://doi.org/10.1016/j.bios.2015.11.087>
7. Zhang L, Fang M (2010) Nanomaterials in pollution trace detection and environmental improvement. *Nano Today* 5:128–142. <https://doi.org/10.1016/j.nantod.2010.03.002>
8. Kretschmann E, Raether H (1968) Radiative decay of non-radiative surface plasmons excited by light. *Z Naturforsch A* 23:2135–2136

9. Jorgenson RC, Yee SS (1993) A fiber-optic chemical sensor based on surface plasmon resonance. *Sensors Actuators B Chem* 12:213–220. [https://doi.org/10.1016/0925-4005\(93\)80021-3](https://doi.org/10.1016/0925-4005(93)80021-3)
10. Slavík R, Homola J, Čtyroký J (1999) Single-mode optical fiber surface plasmon resonance sensor. *Sensors Actuators B Chem* 54:74–79. [https://doi.org/10.1016/S0925-4005\(98\)00314-1](https://doi.org/10.1016/S0925-4005(98)00314-1)
11. Trouillet A, Ronot-Trioli C, Veillas C, Gagnaire H (1996) Chemical sensing by surface plasmon resonance in a multimode optical fibre. *Pure Appl Opt J Eur Opt Soc Part A* 5:227–237. <https://doi.org/10.1088/0963-9659/5/2/006>
12. Zhang XY, Zhang T, Hu AM, Xue XJ, Wu PQ, Chen QY (2011) Tunable Microring Resonator Based on Dielectric-Loaded Surface Plasmon Polariton Waveguides. *J Nanosci Nanotechnol* 11:10520-10524(5). <https://doi.org/10.1166/jnn.2011.4094>
13. Shao LY, Shevchenko Y, Albert J (2010) Intrinsic temperature sensitivity of tilted fiber Bragg grating based surface plasmon resonance sensors. *Opt Express* 18:11464–11471. <https://doi.org/10.1364/OE.18.011464>
14. Schuster T, Herschel R, Neumann N, Schaffer CG (2012) Miniaturized long-period fiber grating assisted surface plasmon resonance sensor. *J Light Technol* 30:1003–1008
15. Chau YFC, Chao CTC, Chiang HP, et al (2018) Plasmonic effects in composite metal nanostructures for sensing applications. *J Nanoparticle Res* 20:190. <https://doi.org/10.1007/s11051-018-4293-4>
16. Kumara NTRN, Chau YFC, Huang JW, et al (2016) Plasmonic spectrum on 1D and 2D periodic arrays of rod-shape metal nanoparticle pairs with different core patterns for biosensor and solar cell applications. *J Opt* 18:115003. <https://doi.org/10.1088/2040-8978/18/11/115003>
17. Russell P (2003) Photonic Crystal Fibres. *Science* 299:358–362
18. De M, Gangwar RK, Singh VK (2017) Designing of highly birefringence, dispersion shifted decagonal photonic crystal fiber with low confinement loss. *Photonics Nanostructures - Fundam Appl* 26:15–23. <https://doi.org/10.1016/j.photonics.2017.06.002>
19. Yang KY, Chau YF, Huang YW, et al (2011) Design of high birefringence and low confinement loss photonic crystal fibers with five rings hexagonal and octagonal symmetry air-holes in fiber cladding. *J Appl Phys* 109:093103. <https://doi.org/10.1063/1.3583560>
20. Rifat AA, Hasan MR, Ahmed R, Butt H (2017) Photonic crystal fiber-based plasmonic biosensor with external sensing approach. *J Nanophotonics* 12:012503-1–10. <https://doi.org/10.1117/1.jnp.12.019901>
21. Momota MR, Hasan MR (2018) Hollow-core silver coated photonic crystal fiber plasmonic sensor. *Opt Mater (Amst)* 76:287–294. <https://doi.org/10.1016/j.optmat.2017.12.049>
22. Rifat AA, Mahdiraji GA, Sua YM, et al (2016) Highly sensitive multi-core flat fiber surface

- plasmon resonance refractive index sensor. *Opt Express* 24:2485.  
<https://doi.org/10.1364/OE.24.002485>
23. Tian M, Lu P, Chen L, Lv C, Liu D (2012) All-solid d-shaped photonic fiber sensor based on surface plasmon resonance. *Opt Commun* 285:1550–1554.  
<https://doi.org/10.1016/j.optcom.2011.11.104>
  24. Luan N, Wang R, Lv W, Yao J (2015) Surface plasmon resonance sensor based on D-shaped microstructured optical fiber with hollow core. *Opt Express* 23:8576–8582.  
<https://doi.org/10.1364/OE.23.008576>
  25. Chen X, Xia L, Li C (2018) Surface Plasmon Resonance Sensor Based on a Novel D-Shaped Photonic Crystal Fiber for Low Refractive Index Detection. *IEEE Photonics J* 10:6800709.  
<https://doi.org/10.1109/JPHOT.2018.2790424>
  26. Dash JN, Jha R (2014) Graphene-Based Birefringent Photonic Crystal Fiber Sensor Using Surface Plasmon Resonance. *IEEE Photonics Technol Lett* 26:1092–1095
  27. Dash JN, Jha R (2015) On the performance of graphene-based D-shaped photonic crystal fibre biosensor using surface plasmon resonance. *Plasmonics* 10:1123–1131
  28. Dutta A, Deka B, Sahu PP (2016) *Planar Waveguide Optical Sensors : From Theory to Applications*. Springer International Publishing, Switzerland
  29. Scott AM, Wang P, Cooper LJ, et al (2005) High-power Yb-doped multicore ribbon fiber laser. *Opt Lett* 30:2906. <https://doi.org/10.1364/ol.30.002906>
  30. Mahdiraji GA, Amirkhan F, Chow DM, Kakaie Z, Yong PS, Dambul KD, Adikan FRM (2014) Multicore Flat Fiber: A New Fabrication Technique. *IEEE Photonics Technol Lett* 26:1972–1974.  
<https://doi.org/10.1109/LPT.2014.2343637>
  31. Egorova O, Astapovich M, Semenov S, Salganskii M (2014) Multicore optical fiber with rectangular cross-section. *Opt Lett* 39:2168–2170. <https://doi.org/10.15593/2411-4367/2016.01.02>
  32. Gangwar RK, Singh VK (2017) Highly Sensitive Surface Plasmon Resonance Based D-Shaped Photonic Crystal Fiber Refractive Index Sensor. *Plasmonics* 12:1367–1372.  
<https://doi.org/10.1007/s11468-016-0395-y>
  33. Search H, Journals C, Contact A, Iopscience M (2015) Infrared SPR sensitivity enhancement using ITO / TiO<sub>2</sub> / silicon. *Europhys Lett* 112:10001-p1-5. <https://doi.org/10.1209/0295-5075/112/10001>
  34. Chau YFC, Chou Chao CT, Lim CM, et al (2018) Depolying tunable metal-shell/dielectric core nanorod arrays as the virtually perfect absorber in the near-infrared regime. *ACS Omega* 3:7508–7516. <https://doi.org/10.1021/acsomega.8b00362>
  35. Aouani H, Wenger J, Gérard D, et al (2009) Crucial role of the adhesion layer on the plasmonic

- fluorescence enhancement. *ACS Nano* 3:2043–2048. <https://doi.org/10.1021/nn900460t>
36. Jiao X, Goeckeritz J, Blair S, Oldham M (2009) Localization of near-field resonances in bowtie antennae: Influence of adhesion layers. *Plasmonics* 4:37–50. <https://doi.org/10.1007/s11468-008-9075-x>
  37. Brückner V (2011) To the use of Sellmeier formula. In: *Elements of optical networking*. Springer, p 217
  38. Johnson PB, Christy RW (1972) Optical constant of the noble metals. *Phys Rev B* 6:4370–4379. <https://doi.org/10.1103/PhysRevB.6.4370>
  39. COMSOL Multiphysics. [www.comsol.com](http://www.comsol.com)
  40. Auguste JL, Humbert G, Leparmentier S, et al (2014) Modified powder-in-tube technique based on the consolidation processing of powder materials for fabricating specialty optical fibers. *Materials (Basel)* 7:6045–6063. <https://doi.org/10.3390/ma7086045>
  41. Armelao L, Barreca D, Bottaro G, et al (2005) RF-sputtering of gold on silica surfaces: Evolution from clusters to continuous films. *Mater Sci Eng C* 25:599–603. <https://doi.org/10.1016/j.msec.2005.06.007>
  42. Pathak AK, Bhardwaj V, Gangwar RK, De M, Singh VK (2016) Fabrication and characterization of TiO<sub>2</sub> coated cone shaped nano-fiber pH sensor. *Opt Commun* 386:. <https://doi.org/10.1016/j.optcom.2016.11.021>
  43. Wei Li, Hu Cheng, Min Xia KY (2013) An experimental study of pH optical sensor using a section of no-core fiber. *Sensors Actuators A Phys* 199:260–264. <https://doi.org/10.1016/j.sna.2014.12.020>
  44. Heng DOZ, An YLI, Hen ERHUC, et al (2016) Free-space to few-mode-fiber coupling under atmospheric turbulence. *Opt Express* 24:18739–18744
  45. Rifat AA, Mahdiraji GA, Ahmed R, et al (2016) Copper-graphene-based photonic crystal fiber plasmonic biosensor. *IEEE Photonics J* 8:4800408. <https://doi.org/10.1109/JPHOT.2015.2510632>
  46. An G, Li S, Yan X, et al (2017) Extra-broad Photonic Crystal Fiber Refractive Index Sensor Based on Surface Plasmon Resonance. *Plasmonics* 12:465–471. <https://doi.org/10.1007/s11468-016-0286-2>